Luminescence properties of mixed-ligand MOFs containing fluorene scaffolds functionalized with isonicotinoyl arms†

Andrea Delledonne, [ID] [a] Martina Orlandini, [a] Francesca Terenziani, [ID] *[a]
Paolo Pio Mazzeo, [ID] [a] Alessia Bacchi, [ID] [a] Lucia Carlucci, [ID] [b] Angiolina Comotti, [ID] [c]
Jacopo Perego [ID] [c] and Paolo Pelagatti [ID] *[ad]

Solvothermal reactions between three bis-pyridine-bis-amide ligands containing a fluorene scaffold bearing different substituents on the C9 position (CH₂, **1**; CMe₂, **2**; C═O, **3**) with 2,6-naphthalenedicarboxylic acid (H₂ndca) and Zn(NO₃)₂·6H₂O led to the isolation of three new microporous mixed-ligand MOFs (**PUM310**, containing **1**; **PUM310Me₂**, containing **2**; **PUM310CO**, containing **3**). The structural characterization conducted with X-ray quality single crystals revealed parallel polycatenated frameworks of thick layers in all cases, corresponding to the topological type 5,6L18. The entangled nets contain complete and truncated Zn-paddle wheels. In the truncated paddle wheel, a pyridine of the bis-amide linker has been replaced by a DMF molecule. Solvent removal leads to framework rearrangement, as evidenced by XRPD analysis performed on desolvated **PUM310**, with consequent framework shrinkage as also evidenced by volumetric adsorption analyses. The three MOFs are fluorescent in the solid state. The optical spectra are indicative of a Förster resonance energy transfer (FRET) involving ndca²⁻ as an excitation energy donor and the bis-pyridine linkers as acceptors, with a FRET efficiency close to 100% in the case of **PUM310CO**.

Introduction

Although more than twenty years have passed since the pioneering work by Yaghi,[1] metal–organic-frameworks (MOFs) are still attracting tremendous scientific interest due to their high crystallinity, high porosity and high modularity.[2–4] MOFs are potentially porous coordination networks composed of metal nodes, often reported as secondary-building-units (SBUs), and polytopic linkers.[5] The crystallinity of MOFs and the knowledge of their precise crystalline structure enable the design of new architectures and the development of new functional materials that make MOFs highly attractive in several applications, such as gas storage and separation,[6–10] guest-inclusion,[11–15] development of electronic materials,[16,17] food[18] and environmental[19] control and heterogeneous catalysis.[20–23] Among the physical properties that can be imparted to MOFs, luminescence covers a prominent role in the development of responsive crystalline materials. Indeed, luminescent MOFs (LMOFs), first reported in 2002,[24] are well documented in the literature as sensors[25–27] or as light emitters[28–32] or for biological applications.[33] Luminescence in MOFs can originate from extended π-conjugated organic linkers used to connect the different SBUs (linker-based fluorescence),[26] or from the metal centers (metal-based fluorescence), when the SBUs are formed by suitable metal clusters[30–32,34–37] or lanthanide ions.[38] Alternatively, MOFs can become luminescent by hosting fluorescent guests into their intrinsically porous structure.[39,40] Several examples of LMOFs are related to mixed-ligand MOFs.[41,42] This class of multicomponent materials is derived from the simultaneous incorporation in the framework of two distinct linkers.[43] It follows a widening of the number of functional groups that can be installed in the framework and, in turn, the number of architectures achievable by synthesis, with the possibility of finely tuning the properties of the final materials.[44–48] In the last years, we have directed our attention to Zn-containing

[a] *Department of Chemical Sciences, Life Sciences and Environmental Sustainability, University of Parma, Parco Area delle Scienze 17/A, 43124 Parma, Italy. E-mail: francesca.terenziani@unipr.it, paolo.pelagatti@unipr.it*

[b] *Department of Chemistry, Università degli Studi di Milano, via Golgi 19, 20133 Milano, Italy*

[c] *Department of Materials Science, University of Milano-Bicocca, via Roberto Cozzi 55, 20125 Milano, Italy*

[d] *Interuniversity Consortium Chemical Reactivity and Catalysis (CIRCC), via Celso Ulpiani 27, 70126 Bari, Italy*

† Electronic supplementary information (ESI) available: ¹H NMR spectra of the digested MOFs, TGA traces of pristine MOFs, ORTEP drawings, XRPD trace of **PUM310** after activation, views of the catenated cubic cages, BET analysis, absorption and emission profiles of H₂ndca and solid state absorption of ligands **1**–**3**. CCDC 2215000–2215002. For ESI and crystallographic data in CIF or other electronic format see DOI: https://doi.org/10.1039/d3ce00087g

mixed-ligand MOFs where one of the two linkers is constituted by a polyaromatic scaffold functionalized with bis-isonicotinoyl arms (Scheme 1), while the other is a linear dicarboxylate linker, such as 4,4′-biphenyldicarboxylate or 2,6-naphthalenedicarboxylate. These MOFs, grouped under the acronym PUM (Parma University Materials), have shown propensity for inclusion of organic guests[49–52] and CO_2 adsorption.[53]

Recently, we have reported on the solution and solid state luminescence properties of the three bis-isonicotinoyl linkers containing fluorene scaffolds **1–3** reported in Scheme 1.[54] The results highlighted that although only the fluorenone derivative **3** was fluorescent in solution, all three linkers were fluorescent in the solid state. This prompted us to use the three linkers for the fabrication of mixed-ligand MOFs to investigate their luminescence properties in the solid state, making a comparison with the free linkers. In this paper, we analyze the results obtained from reacting **1–3** with $Zn(NO_3)_2 \cdot 6H_2O$ and 2,6-naphthalenedicarboxylic acid in *N,N*-dimethylformamide (DMF), under solvothermal conditions. The solid state structures of the three new MOFs (**PUM310**, containing **1**; **PUM310Me$_2$**, containing **2**; **PUM310CO**, containing **3**) and their topologies are described, along with their thermal behavior and luminescence properties in the solid state.

Experimental

Materials and methods

All reagents and solvents were used as received. The bis-pyridyl-bis-amide ligands **1–3** were synthesized as previously reported.[54]
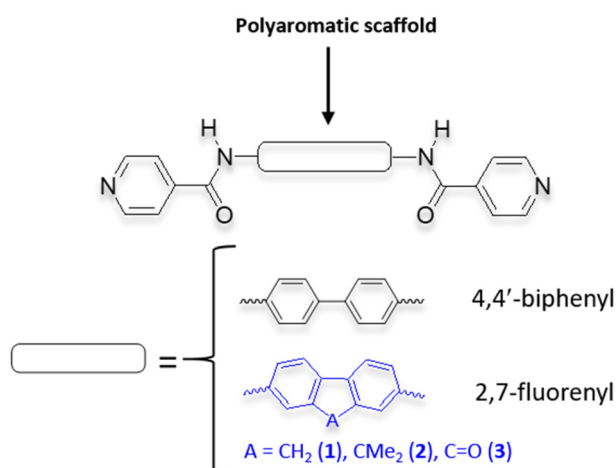
^{1}H NMR spectra were recorded on a 400 or 300 MHz Bruker instrument after dissolution of the materials in one drop of CF_3COOD (TFA) and dilution with $(CD_3)_2SO$ (DMSO). Chemical shifts are reported in ppm relative to the solvent residual peak of deuterated DMSO ([1]H = 2.50 ppm). TGA analyses (sample mass approximately 1–3 mg) were conducted by means of a PerkinElmer TGA8000 instrument, using a Pt-crucible, with a temperature increment of 10 °C min^{-1} in the temperature range of 25–500 °C. The measurements were performed under ambient pressure with a nitrogen gas flow of 80 mL min^{-1}. The maximum temperature was fixed at 500 °C to avoid any damage to the Pt-crucible, due to the presence of metals in the specimen. Elemental analyses were performed using a Thermo Fisher FlashSmart instrument, with gas-chromatographic separation.

Single crystal X-ray diffraction data were collected at Elettra Synchrotron (Trieste, Italy) beamline XRD1.[55] Crystals were directly removed from DMF and data were collected at 100 K using an Oxford Cryostream system. Beamline spectra (produced by an NdBFe multipole wiggler) were monochromatized to 17.71 keV (0.700 Å) through a Si(111) double crystal monochromator and focused to obtain a beam size of 0.2 × 0.2 mm FWHM at the sample (photon flux = 10^{12}–10^{13} ph s^{-1}). Datasets were collected at 100 K (nitrogen stream supplied through an Oxford Cryostream 700) through the rotating crystal method. Diffraction data were indexed, integrated and scaled by using the software CrysAlis.[56] Structures were solved by direct methods using SHELXT[57] and refined by full-matrix least-squares on all F^2 using SHELXL[58] implemented in Olex2.2.[59] For all structures, anisotropic displacement parameters were refined except for hydrogen atoms. Table 1 reports the crystal data collection and refinement results. ORTEP diagrams are reported in the ESI.† Crystallographic data for the reported structures were deposited with the CCDC codes 2215000–2215002.

UV-vis absorption spectra were recorded with a PerkinElmer Lambda650 spectrophotometer; fluorescence measurements were performed with an FLS1000 Edinburgh Instruments Fluorometer. Emission spectra of liquid samples were collected on diluted solutions, with an absorbance lower than 0.1. Solutions for spectroscopic measurements were prepared using spectrophotometric grade or HPLC grade solvents.

The spectroscopic analysis of solid samples required a careful preparation of the specimens: a small quantity of solid was ground in a mortar and then deposited mechanically on a quartz plate, creating an extremely thin layer. For absorption measurements, the samples thus prepared were directly placed into the sample holder of the Lambda 650 spectrophotometer; absorption spectra were collected in transmission mode, with the light beam directed perpendicularly through the sample, using air as a reference. For emission spectra, the thickness of the layers was reduced as much as possible to minimize inner-filter effects, considering the thickness acceptable when the excitation profile of ndca^{2-} (the energy donor) was comparable with the absorption spectrum of pure H_2ndca. In order to prevent the reflected light from propagating along the emission path, a front-face sample holder was used to collect the fluorescence spectra of the thin layers, and was rotated by 45° with respect

Scheme 1 General structure of bis-isonicotinoyl linkers containing different polyaromatic scaffolds. The 2,7-fluorenyl scaffold contained in the linkers used for the construction of the MOFs described in this work is in blue.

Table 1 Crystal data and structure refinement for **PUM310**, **PUM310CO** and **PUM310Me$_2$**

Identification code	PUM310	PUM310CO	PUM310Me$_2$
Empirical formula	$C_{64}H_{43}N_5O_{15}Zn_3\cdot0.5(C_3H_7NO)$	$C_{64}H_{41}N_5O_{16}Zn_3$	$C_{132}H_{93}N_{10}O_{30}Zn_6\cdot3(C_3H_7NO)$
Formula weight	1354.69	1332.13	2910.67
Temperature/K	100(2)	100(2)	100(2)
Crystal system	Monoclinic	Monoclinic	Triclinic
Space group	$P2_1/c$	$P2_1/c$	$P\bar{1}$
a/Å	32.28(6)	31.752(2)	17.6312(7)
b/Å	17.76(3)	17.8208(5)	19.4232(4)
c/Å	19.21(3)	19.1271(8)	31.8390(12)
α/°	90	90	104.948(3)
β/°	104.08(5)	105.392(6)	103.585(3)
γ/°	90	90	90.131(3)
Volume/Å^3	10 685(31)	10 434.8(10)	10 216.7(6)
Z	4	4	2
ρ_{calc}/g cm^{-3}	0.842	0.848	0.946
μ/mm^{-1}	0.710	0.699	0.719
$F(000)$	2768.0	2712.0	2990.0
Crystal size/mm^3	0.08 × 0.06 × 0.02	0.06 × 0.06 × 0.02	0.06 × 0.04 × 0.02
Radiation	Synchrotron (λ = 0.700)	Synchrotron (λ = 0.700)	Synchrotron (λ = 0.700)
2Θ range for data collection/°	4.372 to 59.786	3.454 to 51.888	3.108 to 51.888
Index ranges	$-44 \leq h \leq 44$	$-39 \leq h \leq 39$	$-22 \leq h \leq 22$
	$-24 \leq k \leq 24$	$-22 \leq k \leq 22$	$-23 \leq k \leq 23$
	$-26 \leq l \leq 26$	$-23 \leq l \leq 23$	$-39 \leq l \leq 39$
Reflections collected	461 211	132 861	65 422
Independent reflections	30 220	21 230	38 133
	R_{int} = 0.1433	R_{int} = 0.1371	R_{int} = 0.0410
	R_{sigma} = 0.0703	R_{sigma} = 0.0778	R_{sigma} = 0.0709
Data/restraints/parameters	30 220/62/603	21 230/620/633	38 133/0/1057
Goodness-of-fit on F^2	1.016	1.467	1.512
Final R indices [$I \geq 2\sigma(I)$]	R_1 = 0.1008	R_1 = 0.1563	R_1 = 0.1422
	wR_2 = 0.2929	wR_2 = 0.4290	wR_2 = 0.4017
Final R indices [all data]	R_1 = 0.1671	R_1 = 0.2076	R_1 = 0.1688
	wR_2 = 0.3656	wR_2 = 0.4615	wR_2 = 0.4218
Largest diff. peak/hole/e Å^{-3}	6.20/−1.81	6.01/−2.57	5.09/−2.14

to the excitation beam and tilted off the vertical. Moreover, potential artefacts due to scattering and stray light were removed by employing appropriate longpass filters in the emission path (the cut-off wavelength is indicated in the captions of the figures). Corrections for detector sensitivity and excitation intensity were applied to all the fluorescence and excitation spectra.

N_2 adsorption isotherms at 77 K and CO_2 adsorption isotherms at 195 K were collected up to 1 bar using a Micromeritics analyser ASAP2020 HD.

Synthesis of PUM310, PUM310CO and PUM310Me$_2$

Syntheses of the coordination networks were conducted under solvothermal conditions dissolving **1–3** (0.05 mmol), 2,6-naphthalenedicarboxylic acid (H_2ndca, 0.1 mmol, 21.6 mg) and $Zn(NO_3)_2\cdot6H_2O$ (0.1 mmol, 29.7 mg) in 10 mL of DMF at room temperature in 20 mL screw-capped Pyrex-glass tubes. The mixture was sonicated until complete dissolution of the reagents, then the sealed tube was immersed in a silicon oil bath thermostated at 80 °C, for the time necessary to grow X-ray quality single crystals. Then, the tube was slowly cooled at room temperature, and the crystals were filtered off and washed with DMF (2 × 5 mL). To avoid degradation, the crystals were stored in DMF. Prior to

analysis by ^{1}H NMR and TGA, the crystals were gently passed over a filter paper to remove DMF from the surface of the crystals.

Synthesis of PUM310. Following the general procedure with ligand **1** (40.6 mg), the solution was heated for five days isolating yellow plate crystals. A %weight loss of 27.9% by TGA, in the interval of 30–100 °C, corresponds to 7 molecules of DMF. Decomposition occurs at temperatures of >400 °C. Elemental analysis calculated for $C_{64}H_{43}N_5O_{15}Zn_3\cdot3(DMF)$: C, 57.03 (56.85); H, 4.20 (3.88); N, 7.29 (7.01), indicative of a partial loss of solvent during storage.

Synthesis of PUM310Me$_2$. Following the general procedure with ligand **2** (43.4 mg), the solution was heated for four days isolating yellow plate crystals. A %weight loss of 16.07% by TGA, in the interval of 30–250 °C, corresponds to 7 molecules of DMF; decomposition temperature = >400 °C. Elemental analysis calculated for $C_{132}H_{93}N_{10}O_{30}Zn_6\cdot3(DMF)$: C, 67.24 (66.85); H, 4.56 (4.36); N, 7.23 (7.11), indicative of a partial loss of solvent during storage.

Synthesis of PUM310CO. Following the general procedure with ligand **3** (42.0 mg), the solution was heated for four days isolating orange plate crystals. A %weight loss of 31.09% by TGA, in the interval of 30–250 °C, corresponds to 8 molecules of DMF; decomposition temperature = >400 °C. Elemental analysis calcd for $C_{64}H_{41}N_5O_{16}Zn_3\cdot4(DMF)$: C, 56.19 (56.09);

H, 4.28 (3.98); N, 7.76 (7.51), indicative of a partial loss of solvent during storage.

Results and discussion

Synthesis and structural characterization

The three bis-amide-bis-pyridine ligands **1**–**3** were reacted under solvothermal conditions with 2,6-naphthalenedicarboxylic acid (H$_2$ndca) and zinc nitrate hexahydrate in DMF at 80 °C, as depicted in Fig. 1.

The reactions with **1** and **3** led to the isolation of yellow and orange crystals, corresponding to **PUM310** and **PUM310CO**, respectively. The two MOFs are isostructural, crystallizing in the $P2_1/c$ monoclinic space group. The content of the asymmetric units is very similar, differing only in the DMF content. In both cases, the asymmetric unit contains three independent Zn^{2+} ions, an **L** (**L** = **1** or **3**) ligand, three ndca^{2-} anions and a coordinated DMF molecule. A partially occupied DMF molecule H-bonded to an amide NH group was also observed in **PUM310**. Unmodelled residual electron density is ascribable to disordered molecules of DMF included in the cavities of the frameworks of **PUM310** and **PUM310CO**, respectively. The ^{1}HNMR spectra of the crystals of **PUM310** and **PUM310CO** digested in a mixture of TFA-d and DMSO-d$_6$ indicate the presence of about 10 and 8 molecules of DMF, respectively. TGA analysis showed a weight loss percentage of 27.9% and 31.09% in the interval of 30–250 °C for **PUM310** and **PUM310CO**, respectively, corresponding to the departure of about 7 and 8 molecules of DMF. Although a perfect counting of the DMF molecules is

difficult, we believe that the TGA data are more reliable, and then the general formulae of the two MOFs are [Zn$_3$(**1**) (ndca)$_3$(DMF)]$_n$(DMF)$_6$ and [Zn$_3$(**3**)(ndca)$_3$]$_n$(DMF)$_8$, respectively.

Decomposition of the frameworks occurred at temperatures higher than 400 °C. The reaction with **2** led to **PUM310Me$_2$**, which crystallizes in the $P\bar{1}$ space group and it is isoreticular with **PUM310** and **PUM310CO** (see Fig. 2). The content of the asymmetric unit is higher than in the other two cases due to the space group symmetry. Here in fact, there are six metal nuclei, six ndca^{2-} anions each bridging two Zn^{2+} nuclei, two bis-amide ligands, two coordinated DMF molecules and other three modelled molecules of solvent included in the cavities of the framework.

The ^{1}HNMR spectrum of the crystals of **PUM310Me$_2$** digested in a mixture of TFA-d and DMSO-d$_6$ indicates the presence of approximately 7 molecules of solvent. The approximate general formula is then [Zn$_6$(**2**)$_2$(ndca)$_6$(DMF)$_2$] (DMF)$_5$. The number of DMF molecules was confirmed by TGA analysis with a weight loss percentage of 16.07% in the interval of 30–250 °C. Framework decomposition occurred at temperatures higher than 400 °C. It is worth noting that methyl groups in **2** prevent the net disorder in **PUM310Me$_2$** which is instead evident for **PUM310** and **PUM310CO**. In particular, ligand **3** in **PUM310CO** is heavily disordered with two mutually exclusive orientations of the amide groups, while ligand **1** in **PUM310** keeps the same orientation of the amide groups. Like in other MOFs belonging to the PUM series containing ndca^{2-}, in particular **PUM210** and **PUM210F**,[53] the frameworks of **PUM310** and **PUM310CO**
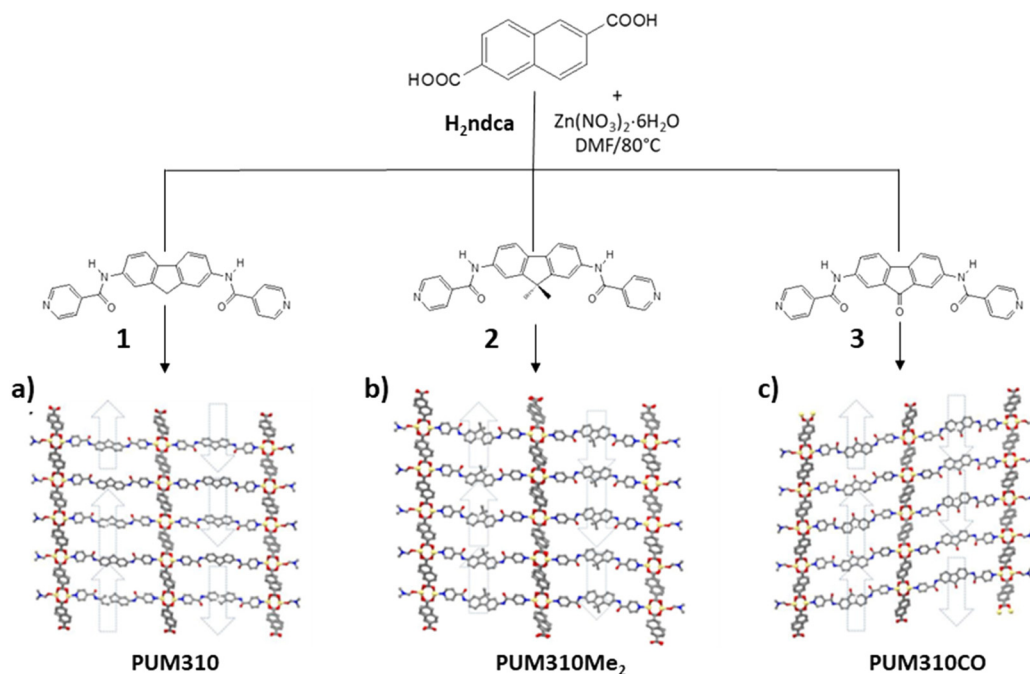

Fig. 1 General scheme of the synthesis of a) **PUM310**, b) **PUM310Me$_2$** and c) **PUM310CO**. For each MOF, the view along the crystallographic *b* axis of the framework is reported, highlighting the reciprocal orientation of the fluorenyl ligand (and the amidic moieties) within the same net. Crystallographic disorder has been removed for the sake of clarity.
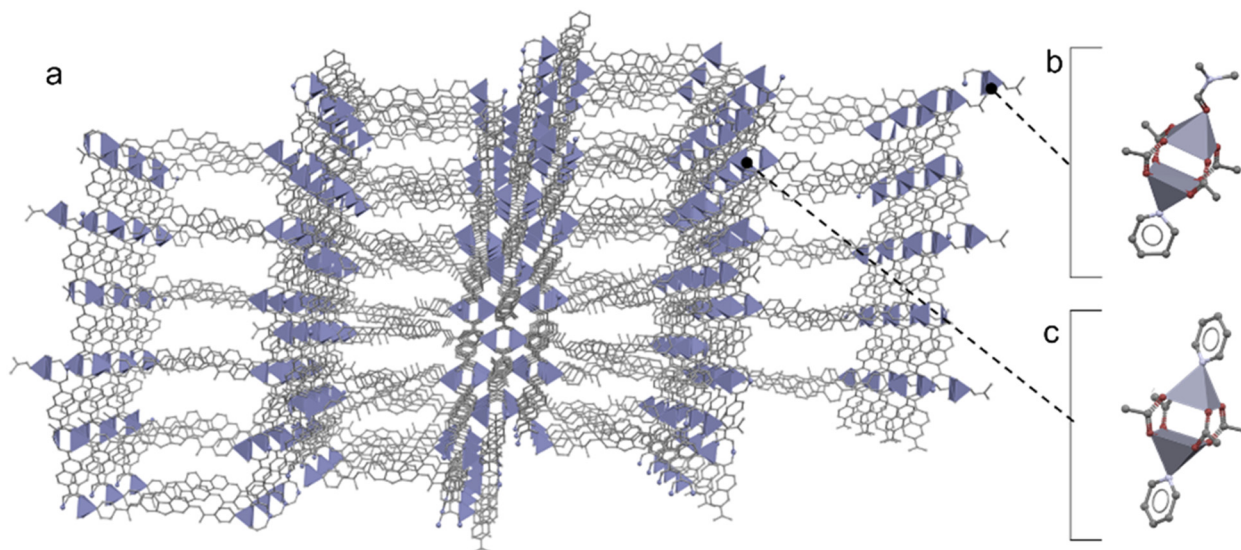
Fig. 2 a) Perspective view of the **PUM310** framework along the crystallographic *b* axis. b and c) Different paddle wheel SBUs are represented as gray polyhedra while the organic ligands are reported in ball and stick style: O: red, N: blue, C: grey.

contain two different SBUs. One is constituted by a complete paddle wheel with the formula $[Zn_2(COO)_4(\mathbf{L})_2]$ (Fig. 2c), where the two metals coordinate four bridged carboxylate groups and two pyridines. The second SBU is a truncated paddle wheel with the formula $[Zn_2(COO)_4(\mathbf{L})(DMF)]$, where an O-coordinated DMF molecule replaces a pyridine (Fig. 2b). The coordinated DMF molecule blocks the framework expansion along the a direction and the pillar motif is then limited to two **L** units (see Fig. 1). The two SBUs are a part of 2D sheets that form planes where the carboxylate ligands lie. These planes are then bridged by **L** linkers. The three structures show polycatenation, analogous to that found in **PUM210F**.[53] **PUM310** shows channels having dimensions of $17.7 \times 12.8 \ \text{Å}^2$, with the void percentage of the unit cell being 24.8%, corresponding to 2648 Å^3 (calculated by the Solvent Accessible Surface function of Mercury), after the removal of disorder. **PUM310CO**, instead, shows channels having a section of 12 Å × 28 Å, with a unit cell void percentage of 24.3% corresponding to 2532 Å^3 (calculated by the Solvent Accessible Surface function of Mercury), after the removal of disorder. Finally, **PUM310Me$_2$** has channels of 13 Å × 19 Å, corresponding to a unit cell void volume of 21.4%, equivalent to 2184 Å^3 (calculated by the Solvent Accessible Surface function of Mercury), after the removal of disorder. Looking at the values of the void volumes of the cells, it turns out that the functionalization of C9 of the fluorenic core translates into a slight decrease of porosity, with **PUM310** featuring the highest void volume.

Framework topology

The three structures reported here are built with 2-periodic 3D layers (2D thick sheets made of three-layers) which are parallel polycatenated (PCAT) to give an overall 3D entangled framework. From a topological point of view, the single thick layers are a binodal 5,6-connected net with point symbol $(4^{12} \cdot 6^3)(4^8 \cdot 6^2)_2$ and correspond to the topological type 5,6L18. They can be seen as a three-layer section of a **pcu** net whose thickness is about 58.6, 57.8 and 55.8 Å for **PUM310**, **PUM310CO** and **PUM310Me$_2$**, respectively (computed by ToposPro[60]). The polycatenation occurs along the direction perpendicular to the thick layers, that is *a* for **PUM310** and **PUM310CO** and *c* for **PUM310Me$_2$**, with an offset approximately equal to the unit cell axis in that direction (*ca.* 32.28, 31.84 and 31.75 Å, respectively). The PCAT arrays in all three structures are characterized by a degree of catenation of 2 (Doc = 2) and an index of separation of 1 (Is = 1), that is, a single multilayer is interlaced with other two, the upper and lower nearest neighbors, and to separate in two halves
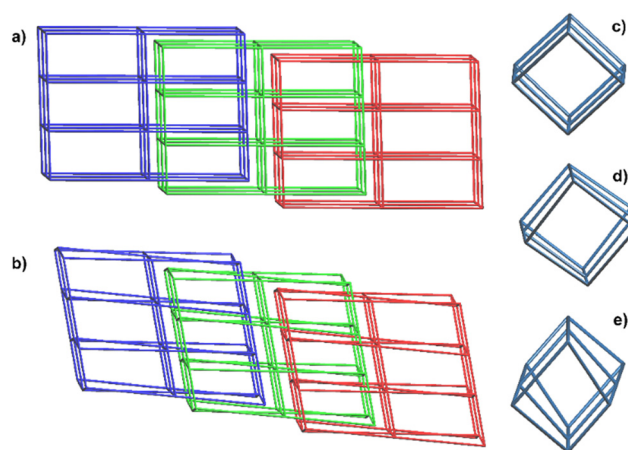

Fig. 3 Views of the simplified networks in (a) **PUM310** and (b) **PUM310Me$_2$** showing the three-layer 2D sheets of the 5,6L18 topology and the parallel polycatenation with Doc = 2 and Is = 1. Shown on the right is the distortion of a single "double-cubic cage" in (c) **PUM310**, (d) **PUM310CO** and (e) **PUM310Me$_2$**.

the whole polycatenated framework, it is necessary to remove just one layer,[61] as shown in Fig. 3.

Results show that each cubic cage of the three-layer **pcu** cut (5,6L18) is interlaced with only one cage of the nearest neighbor layer. Differences between the three structures are related to the degree of distortion of the "double cubic cage" of the thick layers, with the more regular and the more distorted ones found, respectively, in **PUM310** and **PUM310Me₂**, while **PUM310CO** shows only slight distortion (see Fig. 3, right).

This trend seems to follow the steric hindrance of the fluorene scaffold and, as a consequence, the relative arrangement of the ligands in the structures is slightly different (Fig. S10†). The polycatenation shown here (Doc = 2 and Is = 1) is frequently observed for both wavy and thick layers of different topologies;[62,63] however, it is rarely found for layers of the uncommon 5,6L18 topological type.

To the best of our knowledge, this type of thick layer is present in some not polycatenated 2D hybrid perovskites[64–66] and only in two coordination networks previously reported by some of the authors, which are **PUM210F** and **Cu-PUM210F** (CSD refcodes NILFEW and NILFIA[53]). These two networks are strictly related to those reported here, showing the same topology and polycatenation for the layers and differing in the nature of the pillaring ligand (F-bpba). Particularly interesting is the unique structure of **PUM210** (NILFAS), containing the non-fluorinated bpba pillaring ligand, and it has been previously reported together with NILFEW and NILFIA.[53] In this case, the thick 2D motifs are a four-layer **pcu** cut with a thickness of *ca.* 84.13 Å. The corresponding 2-periodic 3D net is 5,6-connected, with point symbol $(4^{12} \cdot 6^3)$ $(4^8 \cdot 6^2)$ and 5,6L48 topology. The polycatenation occurs along the crystallographic ***c*** direction with an offset of about 31.06 Å resulting in Doc = 4 and Is = 2 (see Fig. 4).

As can be seen from Fig. 4, differently from all the other discussed structures, here each cubic cage of a thick layer is interlaced with other two ones belonging to different layers. **PUM210** is the first example of a coordination network with the 5,6L48 topology reported so far, and is one of the few examples of polycatenation with Doc and Is higher than, respectively, 2 and 1. The 5,6L48 topology has only been found in some not entangled 2D hybrid perovskites.[64]

The results discussed here confirm the easy occurrence of parallel polycatenation (PCAT) for 2-periodic 3D layers, such as the multiple pillared layer present in the **PUM** coordination networks. Moreover, the variation of the pillaring ligands in terms of length, steric hindrance and chemical functionalization allows the isolation of new topologies and types of polycatenation.

Stability of the framework upon activation

It is known that for application purposes, MOFs must be activated to remove the solvent molecules included in the cavities of their frameworks.[67] This can be a particularly crucial step since removal of the included solvent can be accompanied by framework collapse with consequent closure of the pores. Due to the similarity of the three isolated frameworks, **PUM310** was chosen as the representative to study the stability of the frameworks towards DMF removal. A close inspection of the TGA curve of **PUM310** shows that 3 molecules of DMF are lost in the *T* range of 25–110 °C (weight loss = 12.15%), while other 3 depart between 110 °C and 210 °C (weight loss = 11.60%). Finally, between 210 °C and 250 °C, a weight loss of 3.96% indicates the departure of an additional DMF molecule. This multistep desolvation profile can be correlated with the increasing degree of interaction between the residual DMF molecules and the framework walls of the MOF. The first loss is ascribed to the departure of the DMF molecules disorderly distributed in the channels, while the other two losses are assigned to the extrusion of the DMF hydrogen-bonded to the framework and coordinated to the Zn of the incomplete SBU, respectively. Thermal activation under dynamic vacuum at a temperature of 100 °C gave severely damaged crystals, not suitable for single-crystal X-ray analysis, thus indicating the need to follow more gentle techniques. For this reason, a solvent-exchange protocol was followed. This involves the soaking of the crystals in two solvents with different low boiling points, such as acetone and dichloromethane. With both solvents, the soaking was maintained for 24 hours. Subsequently, the crystals were evacuated with a simple vacuum at low temperature (see the ESI† for details). The TGA analysis of the activated crystals still showed a weight loss of 10.33%, corresponding to 2.5 molecules of DMF. Most likely, these correspond to the DMF molecules coordinated to zinc and to those strongly interacting with the amide groups of the framework. The activated crystals were subjected to X-ray diffraction analysis, revealing the formation of a new crystalline phase, hereinafter referred to as **PUM310-a**.

The single-crystal-to-single-crystal transformation from **PUM310** to **PUM310-a** was accompanied by a relevant reduction of the cell volume, from 10 682(31) Å³ to 3219(3) Å³, as expected because of the solvent removal. Unfortunately, the framework rearrangement led to damage of the crystals that were no longer suitable for a complete structural resolution. In an attempt to remove completely the included DMF, the soaking times in acetone and dichloromethane were increased to 48 and 72 hours, respectively. The exchanged crystals were then subjected to a heating ramp from 60 °C to 90 °C (within 1 hour). The TGA analysis conducted on the newly activated crystals,
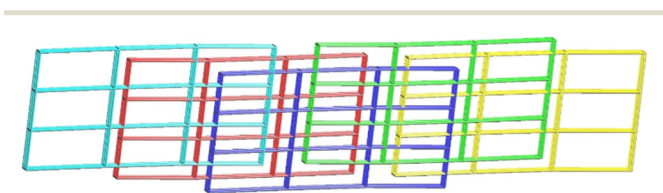

Fig. 4 View of the simplified networks in **PUM210** (NILFAS) showing the four-layer 2D sheets of the 5,6L48 topology and the parallel polycatenation with Doc = 4 and Is = 2.

hereinafter referred to as **PUM310-a′**, showed a weight loss of 5.89%, corresponding to about one molecule of DMF. We assume that the residual DMF corresponds to that contained in the incomplete SBU. Thermal treatment led again to an excessive degradation of the crystals, which were no longer suitable for single crystal X-ray analysis. However, the XRPD trace of **PUM310-a′** is indicative of a new crystalline phase, as inferred by the comparison with the calculated XRPD trace of **PUM310** (see Fig. S11†).

To gain indication of the porosity of the three new MOFs, volumetric adsorption analyses were conducted. Activated **PUM310**, **PUM310Me₂** and **PUM310CO** do not adsorb N_2 at 77 K (see Fig. S12†) whilst a CO_2 uptake at 195 K of 3 mmol g^{-1} (12% weight) was detected for **PUM310-a′** (see Fig. S13†). This value leads to about 4 molecules per asymmetric unit and is significantly lower than the number of DMF molecules initially included, indicating a rearrangement of the framework upon activation, as already anticipated by XRPD analyses, which likely leads to a significant framework shrinkage.

Luminescence

The four organic ligands employed in the synthesis of **PUM310**, **PUM310Me₂** and **PUM310CO** are all fluorescent in the solid state. The spectroscopic properties of **1**, **2** and **3** have been studied in depth in a recent work.[54] The absorption and

emission spectra of the H₂ndca ligand in DMF and in the solid state are reported in the ESI† (Fig. S14).

The three synthesized MOFs have been spectroscopically characterized by recording absorption, emission and excitation spectra directly in the solid state. The fluorescence emission spectra are shown in Fig. 5 together with the ones of the constituting organic ligands. For each MOF, the bands of the two employed ligands, ndca^{2-} and either **1**, **2**, or **3**, can be recognized in the emission spectra. The MOF emission band related to ndca^{2-} is quite similar to the fluorescence spectrum of H₂ndca in DMF, while the emission spectrum of H₂ndca in the solid state is highly affected by aggregate/excimer formation (see the ESI†). This is consistent with the ndca^{2-} ligands being more spaced in the MOF's structure than in the H₂ndca microcrystals. The emission bands of the fluorene-based ligands in **PUM310** and **PUM310Me₂** are almost superimposed and are comparable to those of pure **2** in the solid state, but strongly red-shifted with respect to pure **1**. The emission band of the fluorenone ligand is practically the same as those of **PUM310CO**, **3** as powder and **3** in DMF solution. The large difference between the emission spectra of **PUM310** and **1** as a pure solid can be justified considering the crystal structure of this bis-isonicotinoyl ligand. From the structural data previously reported,[54] molecules are closer in the crystal structure of **1** than in the crystal structure of **2** or in the corresponding MOF. Additionally, several CH–π interactions directly involving the
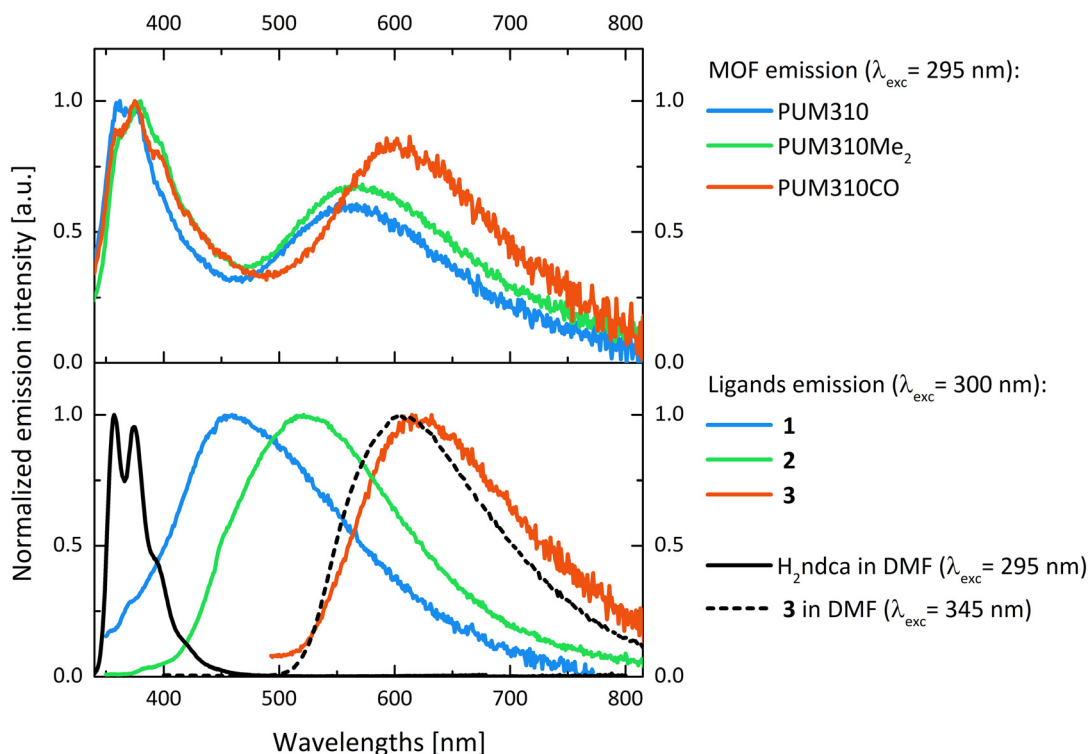

Fig. 5 Comparison between the emission spectra of the three MOFs and of the constituting organic ligands in the solid state (**1**–**3**) or in solution (H₂ndca). Top: Emission spectra of **PUM310**, **PUM310Me₂** and **PUM310CO** in the solid state. Bottom: Emission spectra of H₂ndca and **3** solubilized in DMF and of **1**–**3** in the solid state. All the measurements on the solid samples were performed using a 330 nm longpass filter in the emission path. The excitation wavelength is reported in the legend.
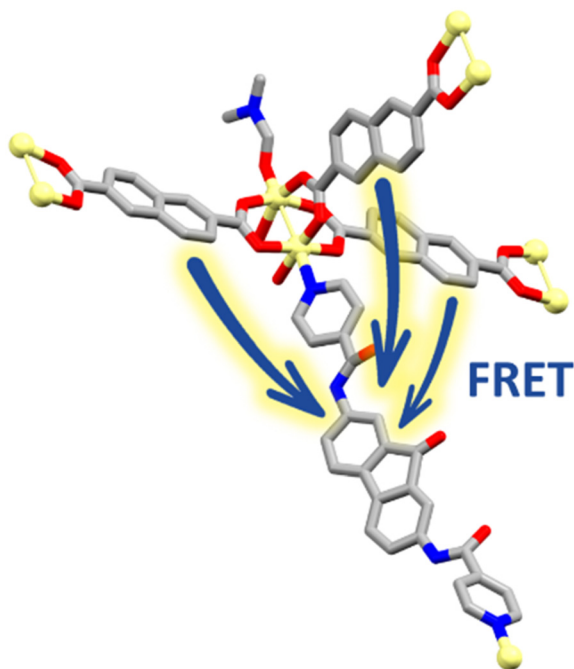
Fig. 6 Partial view of a framework node of **PUM310CO**.

fluorenyl cores were found in the case of pure **1**, which are absent in the structure of **PUM310** and, as expected due to the presence of two methyl groups in position C9, cannot be formed in the case of **2**.

A remarkable complication when measuring fluorescence emission and excitation spectra of solid samples comes from inner filter effects. The primary inner filter effect is related to a very strong absorption of the incident light by the surface

of the sample that prevents the incoming light from reaching the inner parts of the sample; in excitation spectra, this can lead to strong deviations from the absorption profile, even observing minima at the wavelengths where maximum absorption occurs. The second inner filter effect is the self-absorption of the emitted light by the sample itself; this plays a major role when a significant overlap between the emission and absorption spectra is present, and leads to a "spurious" decrease of the emitted intensity in the spectral region overlapping the absorption band. For these reasons, the emission and excitation spectra of solid (or highly concentrated) samples are extremely sensitive to the thickness of the sample. In our measurements on the solid samples, we used extremely thin layers, so inner filter effects were minimized. The absorption spectra of the three MOFs and of the constituent organic ligands are reported in Fig. 7.

Contributions from both ndca^{2-} and the corresponding bis-amide-bis-pyridine ligand are clearly present in the absorption spectra of the three materials. The absorption spectra of ligands **1–3** and the emission spectrum of H$_2$ndca significantly overlap, making them compatible for Förster resonance energy transfer (FRET) (Fig. S15†). Specifically, ndca^{2-} could act as an excitation energy donor, while the three bis-amide-bis-pyridine ligands could act as acceptors. The structure of the MOFs is compatible with FRET, as the two involved ligands are kept in close proximity to each other by the framework structure. In particular, each bis-amide-bis-pyridine ligand can exchange energy with multiple ndca^{2-} located within the same framework (Fig. 6) or in the nearest polycatenated ones.

The selective excitation of the energy donor (ndca^{2-}) is not possible, because of the strong overlap of its absorption bands
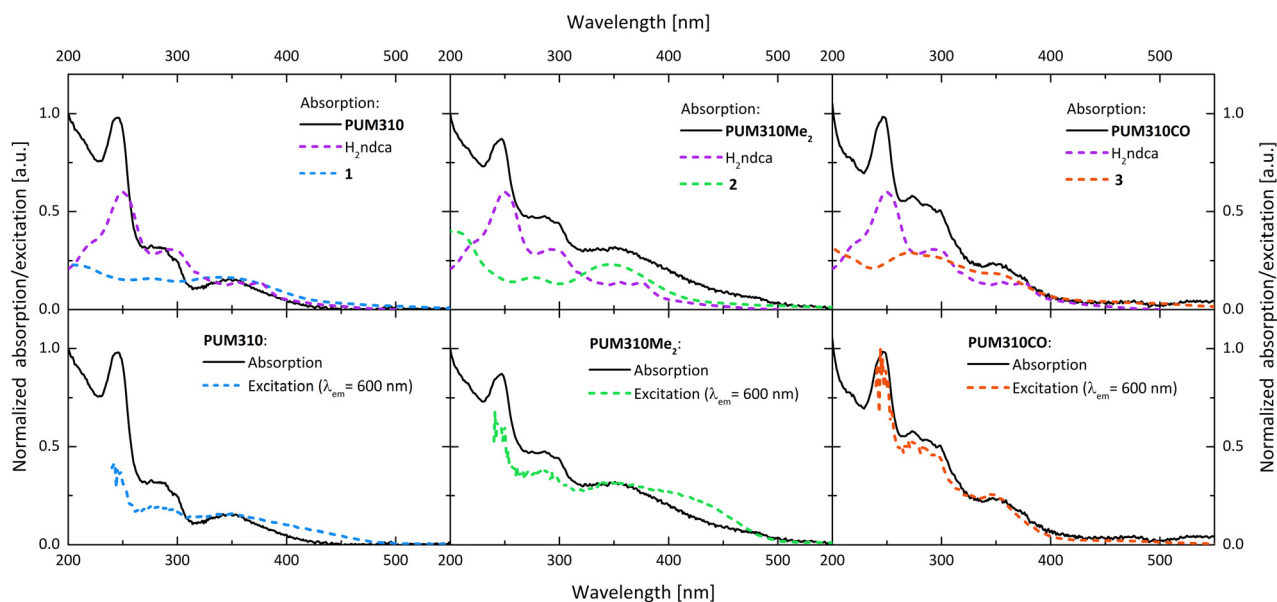

Fig. 7 Top: Comparison between the absorption spectra of **PUM310**, **PUM310Me₂**, **PUM310CO** (continuous black lines), H$_2$ndca (dashed violet lines), **1** (dashed blue line), **2** (dashed green line) and **3** (dashed orange line). Bottom: Comparison between the absorption spectra of **PUM310**, **PUM310Me₂**, and **PUM310CO** and the corresponding excitation spectra obtained collecting the acceptor emission at 600 nm.

with those of the other ligands in the MOFs (Fig. 7, top panels). Therefore, to verify the occurrence of FRET, we acquired the fluorescence excitation spectra of the MOFs while selectively recording the emission from the acceptor ligand (either **1**, **2** or **3**) at 600 nm (Fig. 7, bottom part). The excitation spectra that we obtained for the three MOFs not only display the bands corresponding to the acceptor absorption (either **1**, **2** or **3**), but also display the bands corresponding to the donor absorption (ndca^{2-}; the peak at ~250 nm is very suggestive). In the specific case of **PUM310CO**, the relative intensity of the two contributions is the same as in the corresponding absorption spectrum, suggesting a FRET efficiency close to 100%.

Conclusions

Three new frameworks belonging to the PUM series have been obtained by reacting Zn^{2+} ions with 2,6-naphthalenediacrboxylic acid and three diverse bis-pyridine-bis-amide pillars containing differently functionalized fluorene scaffolds. The type of substituent on the C9 carbon of the fluorene moiety has a little effect on the type of the final framework, and the three MOFs **PUM310**, **PUM310Me₂** and **PUM310CO** are isoreticular. Interestingly, as previously observed by us with other MOFs derived from the combination of 2,6-naphthalenedicarboxylic acid and biphenyl-based bis-pyridine-bis-amide ligands,[53] the frameworks contain two different types of SBUs, corresponding to complete and truncated paddle wheel units. The three-dimensionality is then reached by parallel polycatenation. Although potentially microporous, the flexibility of the frameworks leads to a significant shrinkage of the pores upon desolvation, as evidenced by volumetric adsorption analysis. The framework distortion has been partly followed by X-ray diffraction analysis for **PUM310**, but unfortunately the damage to the crystal during solvent removal has prevented the elucidation of the desolvated structure. The three new MOFs are strongly fluorescent and show FRET from the dicarboxylate dianion to the bis-pyridine linkers, with high efficiencies, close to 100% in the case of **PUM310CO**. These light-harvesting and directional FRET features are promising for multiple sensing applications.

Abbreviations

bpba   Bis-pyridine-biphenyl amide
DMF   N,N-Dimethylformamide
FRET   Förster resonance energy transfer
H₂ndca   2,6-Naphthalenedicarboxylic acid
PUM   Parma University Materials

Author contributions

The manuscript was written through contributions of all the authors. All the authors have given approval to the final version of the manuscript.

Conflicts of interest

There are no conflicts to declare.

Acknowledgements

Notes and references

1 H. Li, M. Eddaoudi, M. O'Keeffe and O. M. Yaghi, *Nature*, 1999, **402**, 276–279.

2 H. C. J. Zhou and S. Kitagawa, *Chem. Soc. Rev.*, 2014, **43**, 5415–5418.

3 S. Kitagawa, R. Kitaura and S.-I. I. Noro, *Angew. Chem., Int. Ed.*, 2004, **43**, 2334–2375.

4 M. Eddaoudi, D. B. Moler, H. Li, B. Chen, T. M. Reineke, M. O'Keeffe and O. M. Yaghi, *Acc. Chem. Res.*, 2001, **34**, 319–330.

5 O. M. Yaghi, M. O'Keeffe, N. W. Ockwig, H. K. Chae, M. Eddaoudi and J. Kim, *Nature*, 2003, **423**, 705–714.

6 R. B. Lin, Z. Zhang and B. Chen, *Acc. Chem. Res.*, 2021, **54**, 3362–3376.

7 G. Cai, P. Yan, L. Zhang, H. C. Zhou and H. L. Jiang, *Chem. Rev.*, 2021, **121**, 12278–12326.

8 L. Meng, K. Liu, S. Fu, L. Wang, C. Liang, G. Li, C. Li and Z. Shi, *J. Solid State Chem.*, 2018, **265**, 285–290.

9 W. Fan, X. Zhang, Z. Kang, X. Liu and D. Sun, *Coord. Chem. Rev.*, 2021, **443**, 213968.

10 S. H. Goh, H. S. Lau and W. F. Yong, *Small*, 2022, **2107536**, 2107536.

11 D. Balestri, D. Capucci, N. Demitri, A. Bacchi and P. Pelagatti, *Materials*, 2017, **10**, 1–12.

12 P. Horcajada, T. Chalati, C. Serre, B. Gillet, C. Sebrie, T. Baati, J. F. Eubank, D. Heurtaux, P. Clayette, C. Kreuz, J. S. Chang, Y. K. Hwang, V. Marsaud, P. N. Bories, L. Cynober, S. Gil, G. Férey, P. Couvreur and R. Gref, *Nat. Mater.*, 2010, **9**, 172–178.

13 J. Vaughn, H. Wu, B. Efremovska, D. H. Olson, J. Mattai, C. Ortiz, A. Puchalski, J. Li and L. Pan, *Chem. Commun.*, 2013, **49**, 5724–5726.

14 P. P. Mazzeo, L. Maini, D. Braga, G. Valenti, F. Paolucci, M. Marcaccio, A. Barbieri and B. Ventura, *Eur. J. Inorg. Chem.*, 2013, 4459–4465.

15 D. Capucci, D. Balestri, P. P. Mazzeo, P. Pelagatti, K. Rubini and A. Bacchi, *Cryst. Growth Des.*, 2017, **17**, 4958–4964.

16   J. Yan, T. Liu, X. Liu, Y. Yan and Y. Huang, *Coord. Chem. Rev.*, 2022, **452**, 214300.

17   N. Kulachenkov, Q. Haar, S. Shipilovskikh, A. Yankin, J. F. Pierson, A. Nominé and V. A. Milichko, *Adv. Funct. Mater.*, 2022, **32**, 1–16.

18   P. L. Wang, L. H. Xie, E. A. Joseph, J. R. Li, X. O. Su and H. C. Zhou, *Chem. Rev.*, 2019, **119**, 10638–10690.

19   F. Bianchi, A. Pankajakshan, F. Fornari, S. Mandal, P. Pelagatti, A. Bacchi, P. P. Mazzeo and M. Careri, *Microchem. J.*, 2020, **154**, 1–7.

20   J. De Tovar, F. Rataboul and L. Djakovitch, *Appl. Catal., A*, 2021, **627**, 118381.

21   Q. Wang, G. Yang, Y. Fu, N. Li, D. Hao and S. Ma, *ChemNanoMat*, 2022, **8**, 1–19.

22   C. G. Piscopo, M. Schwarzer, M. Herrmann, A. Affini, P. Pelagatti, G. Maestri, R. Maggi and S. Loebbecke, *ChemCatChem*, 2016, **8**, 1293–1297.

23   D. Balestri, Y. Roux, M. Mattarozzi, C. Mucchino, L. Heux, D. Brazzolotto, V. Artero, C. Duboc, P. Pelagatti, L. Marchiò and M. Gennari, *Inorg. Chem.*, 2017, **56**, 14801–14808.

24   J. C. Dai, X. T. Wu, Z. Y. Fu, C. P. Cui, S. M. Hu, W. X. Du, L. M. Wu, H. H. Zhang and R. Q. Sun, *Inorg. Chem.*, 2002, **41**, 1391–1396.

25   M. Marimuthu, S. S. Arumugam, D. Sabarinathan, H. Li and Q. Chen, *Trends Food Sci. Technol.*, 2021, **116**, 1002–1028.

26   L. Chen, D. Liu, J. Peng, Q. Du and H. He, *Coord. Chem. Rev.*, 2020, **404**, 213113.

27   F. Fornari, F. Bianchi, N. Riboni, F. Casoli, A. Bacchi, P. P. Mazzeo, P. Pelagatti and M. Careri, *J. Chromatogr. A*, 2022, **1671**, 463010.

28   K. A. White, D. A. Chengelis, M. Zeller, S. J. Geib, J. Szakos, S. Petoud and N. L. Rosi, *Chem. Commun.*, 2009, 4506–4508.

29   R. Li, S. H. Wang, Z. F. Liu, X. X. Chen, Y. Xiao, F. K. Zheng and G. C. Guo, *Cryst. Growth Des.*, 2016, **16**, 3969–3975.

30   L. Maini, D. Braga, P. P. Mazzeo, L. Maschio, M. Rérat, I. Manet and B. Ventura, *Dalton Trans.*, 2015, **44**, 13003–13006.

31   D. Braga, L. Maini, P. P. Mazzeo and B. Ventura, *Chem. – Eur. J.*, 2010, **16**, 1553–1559.

32   F. Farinella, L. Maini, P. P. Mazzeo, V. Fattori, F. Monti and D. Braga, *Dalton Trans.*, 2016, **45**, 17939–17947.

33   A. C. McKinlay, R. E. Morris, P. Horcajada, G. Férey, R. Gref, P. Couvreur and C. Serre, *Angew. Chem., Int. Ed.*, 2010, **49**, 6260–6266.

34   S. Z. Zhan, M. Li, X. P. Zhou, J. H. Wang, J. R. Yang and D. Li, *Chem. Commun.*, 2011, **47**, 12441–12443.

35   D. Braga, F. Grepioni, L. Maini, P. P. Mazzeo and B. Ventura, *New J. Chem.*, 2011, **35**, 339–344.

36   P. P. Mazzeo, L. Maini, A. Petrolati, V. Fattori, K. Shankland and D. Braga, *Dalton Trans.*, 2014, **43**, 9448–9455.

37   L. Maini, D. Braga, P. P. Mazzeo and B. Ventura, *Dalton Trans.*, 2012, **41**, 531–539.

38   J. Rocha, L. D. Carlos, F. A. A. Paz and D. Ananias, *Chem. Soc. Rev.*, 2011, **40**, 926–940.

39   Q. R. Fang, G. S. Zhu, Z. Jin, Y. Y. Ji, J. W. Ye, M. Xue, H. Yang, Y. Wang and S. L. Qiu, *Angew. Chem., Int. Ed.*, 2007, **46**, 6638–6642.

40   J. An, C. M. Shade, D. A. Chengelis-Czegan, S. Petoud and N. L. Rosi, *J. Am. Chem. Soc.*, 2011, **133**, 1220–1223.

41   J. Perego, I. Villa, A. Pedrini, E. C. Padovani, R. Crapanzano, A. Vedda, C. Dujardin, C. X. Bezuidenhout, S. Bracco, P. E. Sozzani, A. Comotti, L. Gironi, M. Beretta, M. Salomoni, N. Kratochwil, S. Gundacker, E. Auffray, F. Meinardi and A. Monguzzi, *Nat. Photonics*, 2021, **15**, 393–400.

42   J. Perego, C. X. Bezuidenhout, I. Villa, F. Cova, R. Crapanzano, I. Frank, F. Pagano, N. Kratochwill, E. Auffray, S. Bracco, A. Vedda, C. Dujardin, P. E. Sozzani, F. Meinardi, A. Comotti and A. Monguzzi, *Nat. Commun.*, 2022, **13**, 1–10.

43   M. Du, C. P. Li, C. Sen Liu and S. M. Fang, *Coord. Chem. Rev.*, 2013, **257**, 1282–1305.

44   S. Pullen and G. H. Clever, *Acc. Chem. Res.*, 2018, **51**, 3052–3064.

45   B. Qin, X. Zhang, J. Qiu, G. Gahungu, H. Yuan and J. Zhang, *Inorg. Chem.*, 2021, **60**, 1716–1725.

46   B. Parmar, K. K. Bisht, Y. Rachuri and E. Suresh, *Inorg. Chem. Front.*, 2020, **7**, 1082–1107.

47   Z. F. Qiu, S. M. Zhao, Z. H. Xu, Y. Zhao, Z. L. Wang and W. Y. Sun, *Cryst. Growth Des.*, 2021, **21**, 5306–5316.

48   S. S. Chen, S. S. Han, C. B. Ma, W. D. Li and Y. Zhao, *Cryst. Growth Des.*, 2021, **21**, 869–885.

49   P. P. Mazzeo, D. Balestri, A. Bacchi and P. Pelagatti, *CrystEngComm*, 2021, **23**, 7262–7269.

50   D. Balestri, P. P. Mazzeo, R. Perrone, F. Fornari, F. Bianchi, M. Careri, A. Bacchi and P. Pelagatti, *Angew. Chem., Int. Ed.*, 2021, **60**, 10194–10202.

51   D. Balestri, P. P. Mazzeo, C. Carraro, N. Demitri, P. Pelagatti and A. Bacchi, *Angew. Chem., Int. Ed.*, 2019, **58**, 17342–17350.

52   D. Balestri, P. Scilabra, C. Carraro, A. Delledonne, A. Bacchi, P. P. Mazzeo, L. Carlucci and P. Pelagatti, *CrystEngComm*, 2019, **21**, 6365–6373.

53   D. Balestri, I. Bassanetti, S. Canossa, C. Gazzurelli, A. Bacchi, S. Bracco, A. Comotti and P. Pelagatti, *Cryst. Growth Des.*, 2018, **18**, 6824–6832.

54   A. Delledonne, M. Orlandini, P. P. Mazzeo, C. Sissa, A. Bacchi, F. Terenziani and P. Pelagatti, *Phys. Chem. Chem. Phys.*, 2022, **24**, 1191–1201.

55   A. Lausi, M. Polentarutti, S. Onesti, J. R. Plaisier, E. Busetto, G. Bais, L. Barba, A. Cassetta, G. Campi and D. Lamba, *Eur. Phys. J. Plus*, 2015, **130**(43), 1–8.

56   *CrysAlisPRO*, Oxford Diffraction/Agilent Technologies, UK Ltd, Yarnton, England, 2008.

57   G. M. Sheldrick, *Acta Crystallogr., Sect. A: Found. Crystallogr.*, 2015, **71**, 3–8.

58   G. M. Sheldrick, *Acta Crystallogr., Sect. C: Struct. Chem.*, 2015, **71**, 3–8.

59   O. V. Dolomanov, L. J. Bourhis, R. J. Gildea, J. A. K. Howard and H. Puschmann, *J. Appl. Crystallogr.*, 2009, **42**, 339–341.

60   V. A. Blatov, A. P. Shevchenko and D. M. Proserpio, *Cryst. Growth Des.*, 2014, **14**, 3576–3586.

61   L. Carlucci, G. Ciani and D. M. Proserpio, *Coord. Chem. Rev.*, 2003, **246**, 247–289.

62 L. Carlucci, G. Ciani, D. M. Proserpio, T. G. Mitina and V. A. Blatov, *Chem. Rev.*, 2014, **114**, 7557–7580.

63 E. V. Alexandrov, V. A. Blatov and D. M. Proserpio, *CrystEngComm*, 2017, **19**, 1993–2006.

64 X. Li, J. Hoffman, W. Ke, M. Chen, H. Tsai, W. Nie, A. D. Mohite, M. Kepenekian, C. Katan, J. Even, M. R. Wasielewski, C. C. Stoumpos and M. G. Kanatzidis, *J. Am. Chem. Soc.*, 2018, **140**, 12226–12238.

65 Z. Xu, W. Weng, Y. Li, X. Liu, T. Yang, M. Li, X. Huang, J. Luo and Z. Sun, *Angew. Chem., Int. Ed.*, 2020, **59**, 21693–21697.

66 L. Li, X. Liu, C. He, S. Wang, C. Ji, X. Zhang, Z. Sun, S. Zhao, M. Hong and J. Luo, *J. Am. Chem. Soc.*, 2020, **142**, 1159–1163.

67 J. E. Mondloch, O. Karagiaridi, O. K. Farha and J. T. Hupp, *CrystEngComm*, 2013, **15**, 9258–9264.